Data Repository 2009040

Mantle weakening and strain localization: Implications for the long-term strength of the continental lithosphere

Jacques Précigout*, Frédéric Gueydan

TABLE. DR1: Constant and parameter values used to construct the lithosphere strength profiles. B: Flow laws and creep parameters of the four olivine deformation mechanisms from Goetze (1978) and Hirth and Kohlstedt (2003). These flow laws are used to construct the deformation map displayed in Figure 1B (Drury, 2005; Precigout et al., 2007).

A Strength profile

Overall parameters

	Crust	Mantle
[1]ρ-Rock density ($kg.m^3$)	2800	3330
[1]Thermal conductivity ($W.m^{-1}.K^{-1}$)	2,5	3,0
Thickness (m)	30000	-

g-Gravitational acceleration ($m.s^{-2}$)	9,81
R-Universal gas constant ($J.mol^{-1}.K^{-1}$)	8,314
$\dot{\varepsilon}$-Overall strain rate (s^{-1})	1.10^{-15}

[1]Crustal Radioactive heat production ($W.m^{-3}$)

$$r = r0.\exp(-z/Hr)$$

With $r0$ ($W.m^{-3}$) = $2{,}565.10^{-6}$; z (m) = depth; Hr (m) = 10000

[1]Burov and Watts (2006)

Brittle rheology

[2]Strength (MPa)

$$\tau_{brittle} = \frac{(2.\mu.\rho.g.z).(1-\lambda)}{(\mu^2+1)^{1/2}+\mu}.10^{-6}$$

With μ (sliding coef.) = 0,6; λ (pore pressure) = 0.

Ductile rheology

Strength (MPa)

1. $\tau_{ductile\,(<200Mpa)} = \dot{\varepsilon}^{(1/n)}.A^{(-1/n)}.\exp[Q/(n.R.T)]$
2. $\tau_{ductile\,(>200Mpa)} = [1-(\ln(A/\dot{\varepsilon}).R.T/Q)^{(1/n)}].8500$

With T in Kelvin and		A ($MPa^{-n}.s^{-1}$)	Q ($J.mol^{-1}$)	n
[1]Crust (wet quartzite)	(equation 1)	$1{,}1.10^4$	223.10^3	4
Mantle (olivine)	[3]< 200MPa	$1{,}1.10^5$	530.10^3	3,5
	[4]> 200MPa	$5{,}7.10^{11}$ (s^{-1})	535.10^3	2

[2]Ranalli (2000) [3]Hirth and Kohlstedt (2003) [4]Goetze (1978)

B Deformation map

Flow laws

For $\tau < 200$ Mpa [1] $\dot{\varepsilon} = \dot{\varepsilon}_r + \dot{\varepsilon}_d + \dot{\varepsilon}_g$

with $\dot{\varepsilon}_{r/d/g} = A_{r/d/g}.\exp[-Q/R.T].\tau^{n_{r/d/g}}.d^{-m_{r/d/g}}$

For $\tau > 200$ Mpa [3] $\dot{\varepsilon} = \dot{\varepsilon}_r + \dot{\varepsilon}_d + \dot{\varepsilon}_g + \dot{\varepsilon}_e$

with [2] $\dot{\varepsilon}_e = A_e.\exp[-(Q/R.T).(1-\tau/\tau_p)^{n_e}]$

Parameters	A ($MPa^{-n}.s^{-1}$) pre-exponential constant	Q ($J.mol^{-1}$) Activation energy	n Stress exponent	m Grain size exponent	τ_p Goetze's constant
[1](Dry)-Dislocation creep (r)	$1{,}1.10^5$	530.10^3	3,5	-	-
[1](Dry)-Diffusion creep (d)	$1{,}5.10^9$	375.10^3	1	3	-
[1]DryGBS creep (g)	$6{,}5.10^3$	400.10^3	3,5	2	-
[2]Exponential creep (e)	$5{,}7.10^{11}$ (s^{-1})	535.10^3	2	-	8500

[1]Hirth and Kohlstedt (2003) [2]Goetze (1978) [3]Drury (2005)

FIGURE DR1.

MODELING RESULTS. 1-D numerical results at three different temperatures (800 °C, 700 °C and 600 °C, from top to bottom) that show first, the highest strain rate recorded within the sheared rock as a function of strain, second, a deformation map at a given temperature, and third, both grain size and strain rate distributions within the sheared rock at five strain steps. The stress/grain size path of the olivine aggregates with the highest strain rate was plotted on the deformation maps in order to document the controlling deformation mechanism during dynamic recrystallization. The mean grain size and strain rate of the five strain steps are also reported in the deformation maps and the strain rate-strain curves. The 1D numerical model was performed using the "finite-difference approximation" for the sheared rock divided into 800 nodes. One node represents an olivine aggregate that is mainly deformed by either dislocation creep, diffusion creep, dryGBS creep or exponential creep, according to its mean grain size, strain rate and shear stress. During the experiment, the strain rate/stress and grain size were thus calculated at each node based on the mechanical equilibrium (constant shear stress throughout the rock). The initial strain rate through the mantle rock was set to 10^{-15} s^{-1} and the results are displayed as dimensionless. The initial grain size distribution throughout the mantle rock is characterized by a random grain size averaged at 3 mm with a standard deviation of 375 μm (Figure A2, strain step t_0). A: Modeling results at 800 °C. A1: Time evolution of the maximum strain rate recorded, to which we added five strain steps (colored dots at 0, 0.4, 0.8, 1.2 and 1.6 strain), in order to illustrate the evolution of both grain size and strain rate distributions in the rock. A2: Distributions of both the mean grain size and the strain rate of all of the olivine aggregates. Such distributions are displayed for the five aforementioned strain steps according to their own specific color. These results show that the deformation of the olivine aggregate at 800 °C is never accommodated by dryGBS creep during dynamic grain size reduction. As a consequence, the GBS-induced weakening does not occur and there is not a local increase in strain rate, i.e. there is no strain localization (fig.A2). B: Modeling results at 700 °C. Unlike the results at 800 °C, some of the olivine aggregates (the smallest) become dominated by dryGBS creep during their mean grain size reduction (deformation map in B1). As a consequence, some weakening occurs during dynamic recrystallization and strain localization is triggered, i.e. one major peak in strain rate within a thin area of the sheared rock (step t_3 in B2) is observed between strain steps t_2 and t_3 (B1). The mean grain size in this forming shear zone then rapidly reaches the balance of the recrystallized grains (deformation map in B1), involving several olivine aggregates with 100% of recrystallized grains (B2). Thus, dynamic recrystallization is complete in these aggregates, leading to the inhibition of the strain localization process in this area and to the redistribution of the strain rate throughout the rock (step t_3 to t_4 in B2). This feature explains the decrease in strain rate within the shear zone that occurs at the end of the experiment, between strain steps t_3 and t_4. C: Modeling results at 600 °C. The dominance of exponential creep on the olivine aggregates during the early stage of deformation (strain steps from t_0 to t_2 in C1) delays the strain localization process, which affects the smallest mean grain size. Despite this feature, the weakening implied by dryGBS creep for the recrystallized grains is larger than the weakening at 700 °C and thus promotes a higher local strain rate increase, i.e. the strain rate has increased by a factor of 50 within a single node at strain step t_3 (C2). As a consequence, the width of this shear zone that localizes strain is thinner than that at 700 °C (B2 and C2).

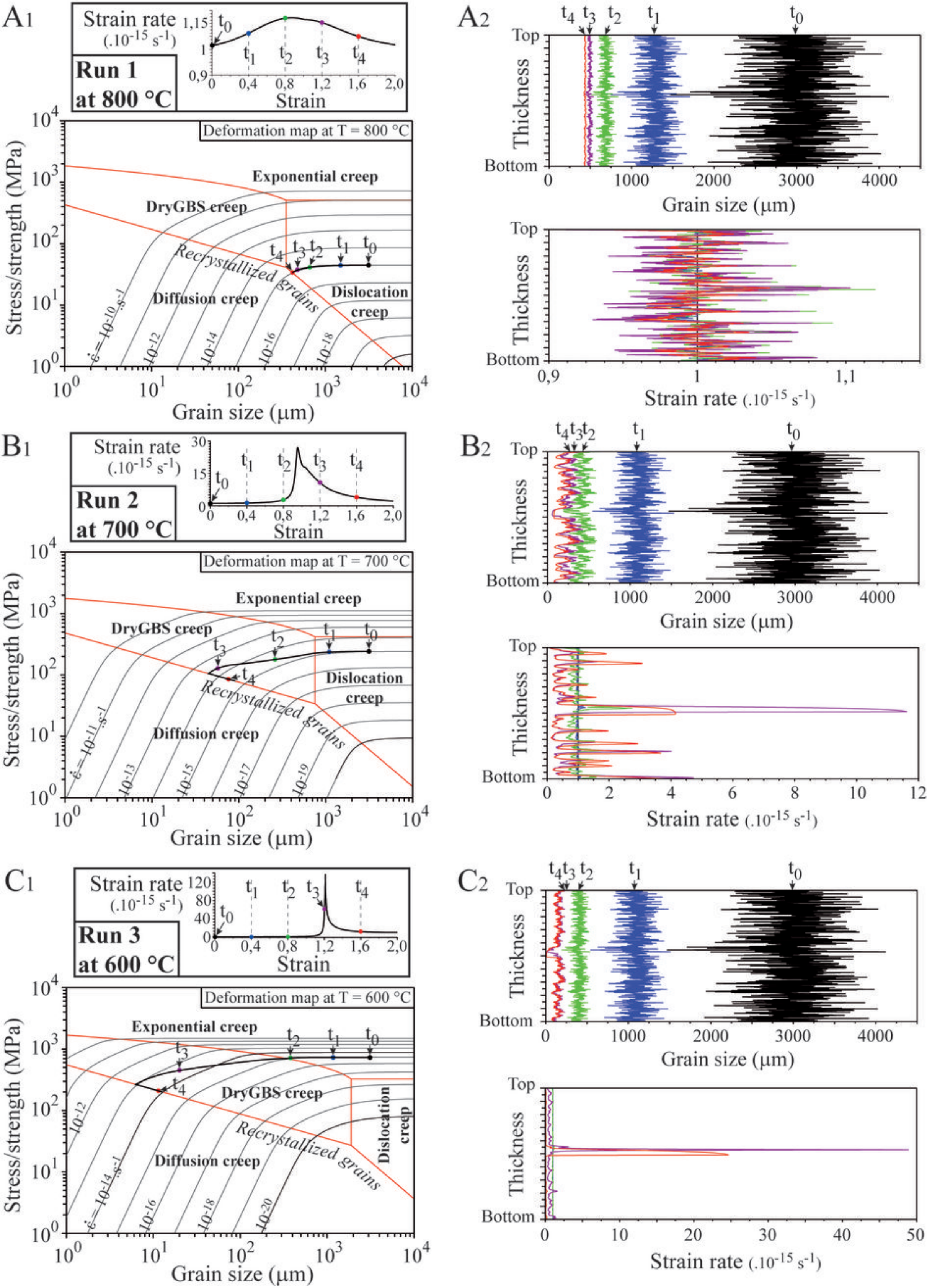

A1
Run 1
at 800 °C
Strain rate (.10-15 s-1)
Strain
t0 t1 t2 t3 t4
Deformation map at T = 800 °C
Exponential creep
DryGBS creep
Recrystallized grains
Diffusion creep
Dislocation creep
Stress/strength (MPa)
Grain size (μm)
A2
Top
Bottom
Thickness
Grain size (μm)
Strain rate (.10-15 s-1)
B1
Run 2
at 700 °C
Strain rate (.10-15 s-1)
Strain
Deformation map at T = 700 °C
Exponential creep
DryGBS creep
Dislocation creep
Recrystallized grains
Diffusion creep
Stress/strength (MPa)
Grain size (μm)
B2
Thickness
Grain size (μm)
Strain rate (.10-15 s-1)
C1
Run 3
at 600 °C
Strain rate (.10-15 s-1)
Strain
Deformation map at T = 600 °C
Exponential creep
DryGBS creep
Dislocation creep
Recrystallized grains
Diffusion creep
Stress/strength (MPa)
Grain size (μm)
C2
Thickness
Grain size (μm)
Strain rate (.10-15 s-1)